Journal of Advanced Biomedical and Pharmaceutical Sciences

JABPS

Journal
Of Advanced Biomedical
And Pharmaceutical Sciences

Design, Synthesis, Molecular Docking and Biological Evaluation of Novel 1,5-Diarylpyrazole-N,O-Dimethyl Hydroxamate Derivatives as Antiproliferative agents

Kamal S. Abdelrahman[1], Heba A. Hassan[2*], Salah A. Abdel-Aziz[1,3], Adel A. Marzouk[1], Raef shams[4], Misato Tajiri[5], Mohamed Abdel-Aziz[2]. Hiroyuki Konno[5]

[1] Department of Pharmaceutical Chemistry, Faculty of Pharmacy, Al-Azhar University, Assiut Branch, Assiut 71524, Egypt

[2] Department of Medicinal Chemistry Faculty of Pharmacy, Minia University, Minia 61519, Egypt

[3] Department of Pharmaceutical Chemistry, Faculty of Pharmacy, Deraya University, Minia, Egypt

[4] Emergent Bioengineering Materials Research Team, RIKEN Centre for Emergent Matter Science, RIKEN, Wako, Saitama 351-0198, Japan

[5] Graduate School of Science and Engineering, Yamagata University, Yonezawa, Yamagata 992-8510, Japan.

Abstract

A series of novel hybrid of 1,5-diarylpyrazole-*N,O*-dimethylhydroxamate derivatives were designed and synthesised in synthetically acceptable yields. All the new synthesized compounds were biologically evaluated for their *in vitro* cytotoxicity against a panel of five cell lines namely human colorectal adenocarcinoma cell line DLD1, human cervical cancer cell line Hela, human leukemia cell line K562, human pancreatic cancer cell line Suit-2 and human hepatocellular carcinoma cell line HepG2. Compound **7a** showed a significant cytotoxicity against Hela cell line with IC_{50} value of 16 µM and a good cytotoxicity against DLD1 and HepG2 with IC_{50} values of 69.9 µM and 78.8µM. Also, compound **7a** displayed a potent EGFR inhibitory activity with $IC_{50} = 4.00$ µM, which was comparable to positive reference drug **sorafenib** ($IC_{50} = 3.5$ µM). Moreover, in-silico studies showed that compound **7a** has excellent binding affinity to the active site of EGFR with binding score better than a multitarget kinase drug **sorafenib** and good binding affinity to JNK-2, which explains the anticancer activity of compound **7a.**

Keywords
Pyrazole; hydroxamate; Cancer; EGFR, Jnk-2.

1. Introduction

Cancer is a significant cause of death worldwide. Hence, the incidence rate of cancer mortality is becoming of global importance[1]. Chemotherapy using drugs that target cell division and angiogenesis or those that induce cancer cell death through different signaling pathways is one of the strategies for treating cancer. However, due to the side effects of chemotherapy and the development of drug resistance in cancer cells, there is a need for design, synthesis and development of effective and safe chemotherapy [2]. EGFR is a tyrosine kinase receptor that plays an important role in cellular signaling activities including cell growth, division, differentiation, metabolism, adhesion and deathdeath[3]. Four tyrosine kinase-related receptors (EGFR, HER2, HER3, and HER4), which have been classified into the HER family. Deregulation of HER family signals enhances proliferation, invasion, metastasis, angiogenesis, and cancer cell survival. Therefore, EGFR receptors are over-expressed in different human tumors such as breast, ovarian, prostate, colon, renal and non-small cell lung cancer (NSCLS)[4-7]. Thus, EGFR inhibition has been developed as one of the most efficient strategies for cancer therapy and several small molecules targeting EGFR are now clinically available such as gefitinib, erlotinib, Lapatinib and Dacomitinib[8].

Pyrazoles are an important class of heterocyclic compounds and exhibit broad range of biological activities including anti-inflammatory, antimicrobial, antioxidant, and anticancer activities[9-11]. Biological evaluation indicated that some pyrazole containing compounds exhibited antiproliferative activity against human cervical cancer cell line Hela by inhibition of Hela cell migration and potent EGFR tyrosine kinase inhibitory activity such as compounds **I**, **II**, **III, IV** and **V (Fig 1)** with IC_{50} values of 0.07, 0.24, 0.06, 0.26 and 0.12 µM, respectively in comparison to a positive control erlotinib ($IC_{50} = 0.03$ µM). Structural activity relationship (SAR) of these pyrazole containing compounds showed that the antiproliferative activity was affected by ring substitution ($OCH_3 > CH_3 > Br > Cl > F$) and compound **V**, which have a naphthalene ring exhibited a highest antiproliferative activity against Hela cell line with IC_{50} value of 0.86 µm as well as a potent EGFR inhibitory activity due to two *p*-π binding of naphthalene ring into EGFR binding site, which enhanced antitumor activity[12].

* *Correspondence: Heba* A *. Hassan*
Tel.: +201068390918;
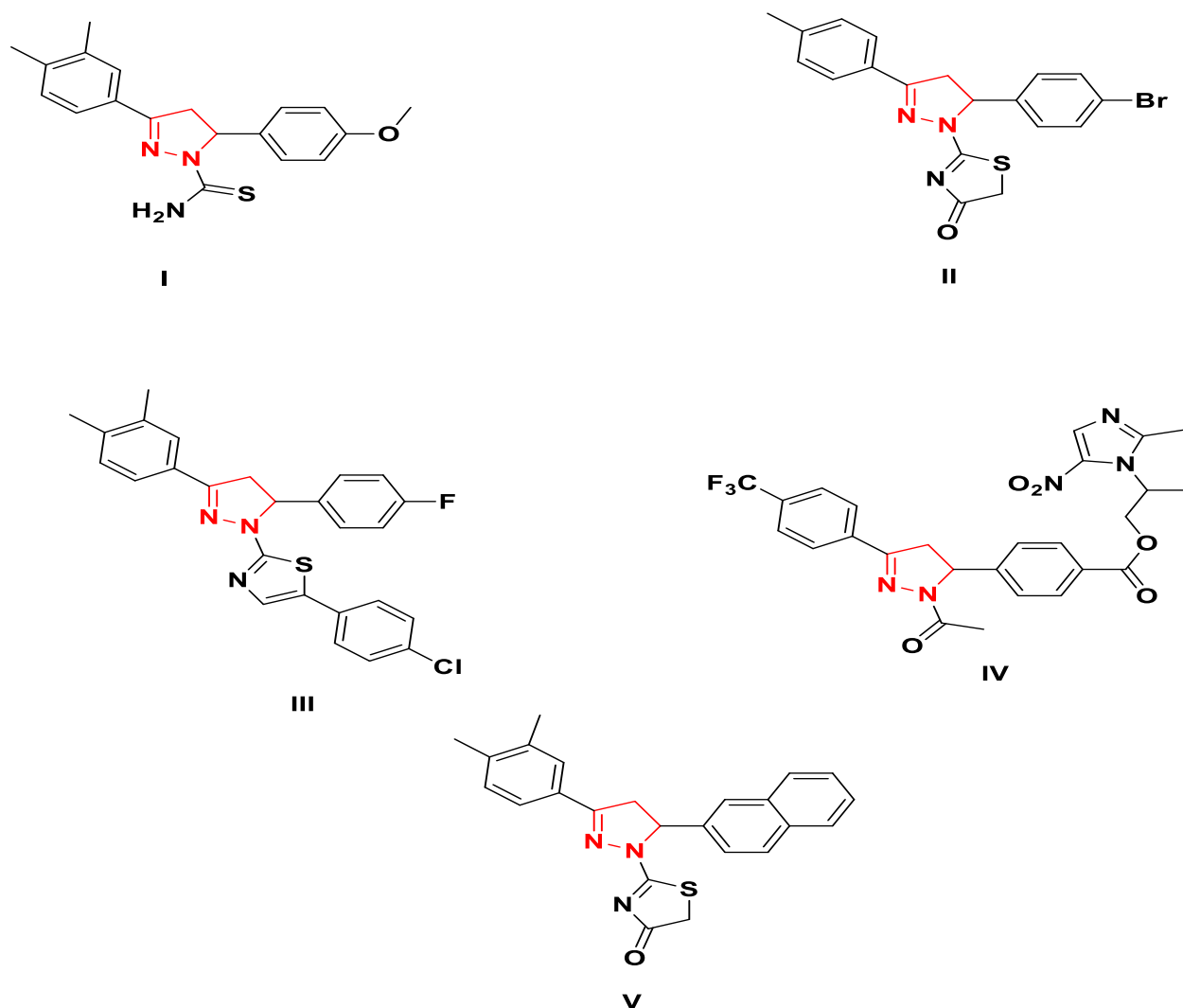*Email Address: heba.hasan@mu.edu.eg*

Figure 1: Structure of pyrazoles I-V with EGFR inhibitory activity.

JNK-2 is a member of MAP kinases family involved in signaling pathways which has been implicated in several diseases like cancer and inflammatory diseases[13]. So, this family is widely considered for targeting by small molecule therapeutics[14].Based on the mode of action of compounds that act as JNK inhibitors, two main categories were found; ATP-competitive inhibitors, which compete with JNK substrates at ATP binding site and inhibit JNK activity and ATP-non-competitive inhibitors, which prevent protein–protein interaction between JNKs and JNK interacting protein JIP or with upstream kinases or the downstream substrates and inhibit JNK activity with little effect on other MAPKs[15]. Biological evaluation of some diarylpyrazole containing compounds revealed that selective COX-2 inhibitor compound **SC-236** showed antitumor activity through blocking of tumor promotor-induced activator protein-1 (AP1) activation as result of suppression of JNK expression[16]. Moreover, compounds **SC74102** and **SC79659** displayed JNK-2 inhibitory activity with IC$_{50}$ of 1.35 and 2.75 µ mol/l respectively, as well as there p38 α inhibitory activity[17](**Fig 2**).

On the other hand, pharmacophore hybridization to synthesize new bioactive compounds is an effective strategy to avoid cancer resistance, which leads to therapeutic failure. Hybridization of two different bioactive molecules with complementary pharmacological functions or with different working mechanisms often shows improved effects[18]. Hybridization of hydroxamic acid or hydroxamic acid derivatives was reported to have different biological activities such as hybridization of hydroxamic acid containing drugs with another anticancer drugs such as rhein-suberoylanilide (SAHA) hybrid, stilbene-SAHA hybrid, nitrogen mustard-vorinostate hybrid and colchicine-vorinostat hybrid, which leads to improve their anticancer efficacy through there dual mechanisms of action[19, 20].(**Fig. 3**.

Depending on the above-mentioned observations on the importance of pyrazole ring as anti-cancer candidate through their effect on EGFR kinases and the importance of hybridization on potentiation of biological activity of some synthetized compounds; this research aims at synthesizing new 1,5-diarylpyrazole hydroxamate derivatives and investigate their anticancer activities.
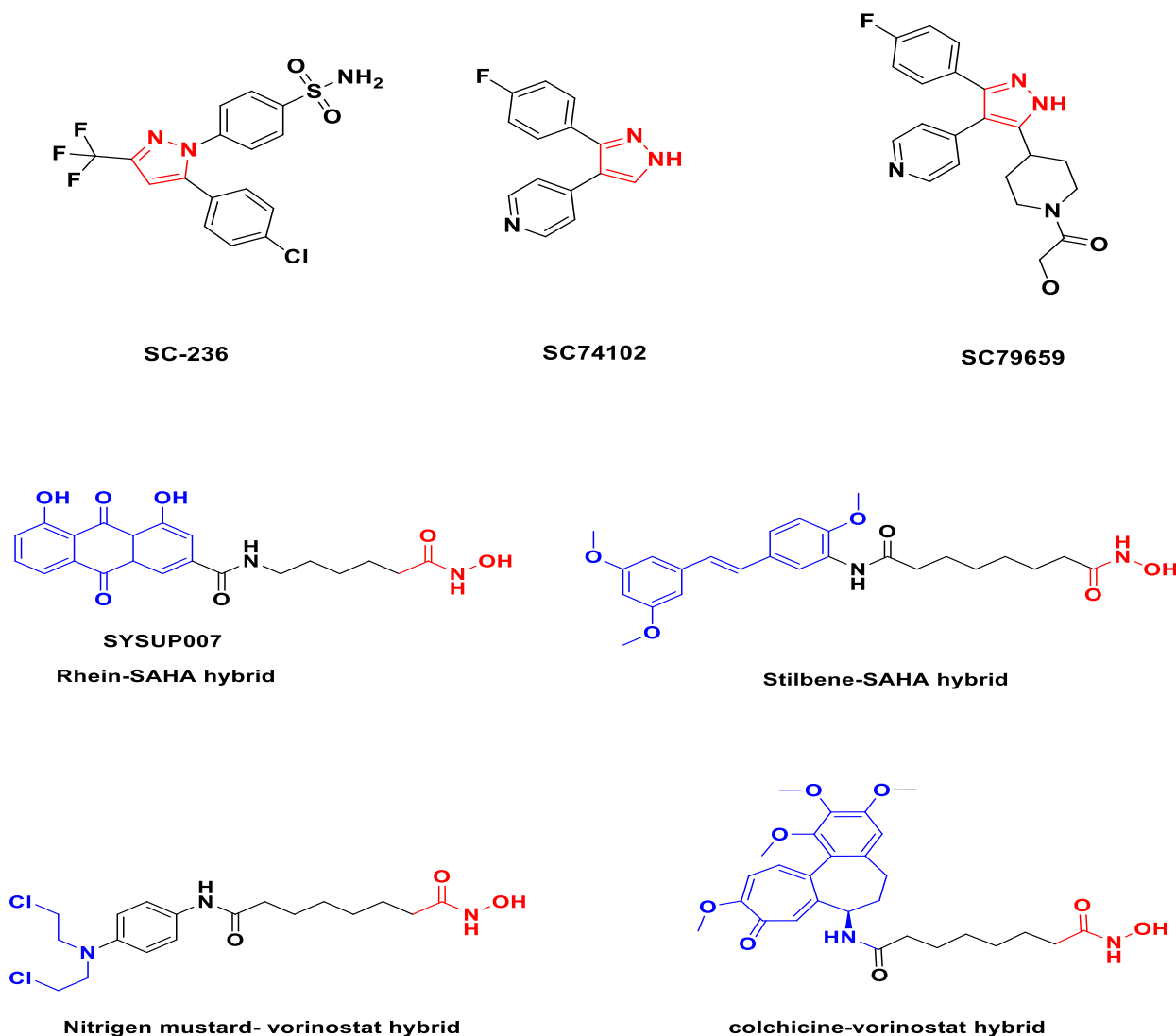
Figure 3: Structure of rhein-SAHA hybrid, stilbene-SAHA hybrid, nitrogen mustard-vorinostate hybrid and colchicine-vorinostat hybrid.

2.Result and Discussion

2.1. Chemistry

The synthetic route used for the preparation of pyrazole acid **6a-f** is illustrated in **Scheme1**. Reaction of acetophenone derivatives **1** with diethyloxalate in the presence of sodium ethoxide yielded 1,3 diketones derivatives **2** with good yield (60-80%). Phenyl hydrazine derivatives **4** were prepared by diazotization of aniline derivatives **3** with sodium nitrite in presence of HCl followed by reduction using sodium sulphite in the presence of sodium hydroxide[21]. Subsequently, compound **2** was refluxed with phenylhydrazine derivatives **4** in the presence of sodium acetate and absolute ethanol to give pyrazole ethyl ester derivatives **5a-f.**

Then saponification of pyrazole ethyl ester derivatives with sodium hydroxide gave pyrazole acid derivatives **6a-f.** Finally, pyrazole acid derivatives **6a-f** were reacted with *N,O*-dimethyl hydroxyl amine in presence of 1-Ethyl-3-(3-dimethylaminopropyl) carbodiimide hydrochloride (EDC), hydroxy benzotriazole (HOBT), were stirred in 5 ml dry DMF for 30 min then *N,N*-diisopropylethylamine (DIPEA) to produce pyrazole carboxamide derivatives **7a-f** [22]**.** The structure of newly synthesized compounds **7a-f** was confirmed by IR, ^{1}H-NMR, ^{13}C and high- resolution mass spectroscopy, **Scheme1.**

R_1= H, 4-OMe, 3,4-OCH$_3$
R_2= H, SO$_2$NH$_2$
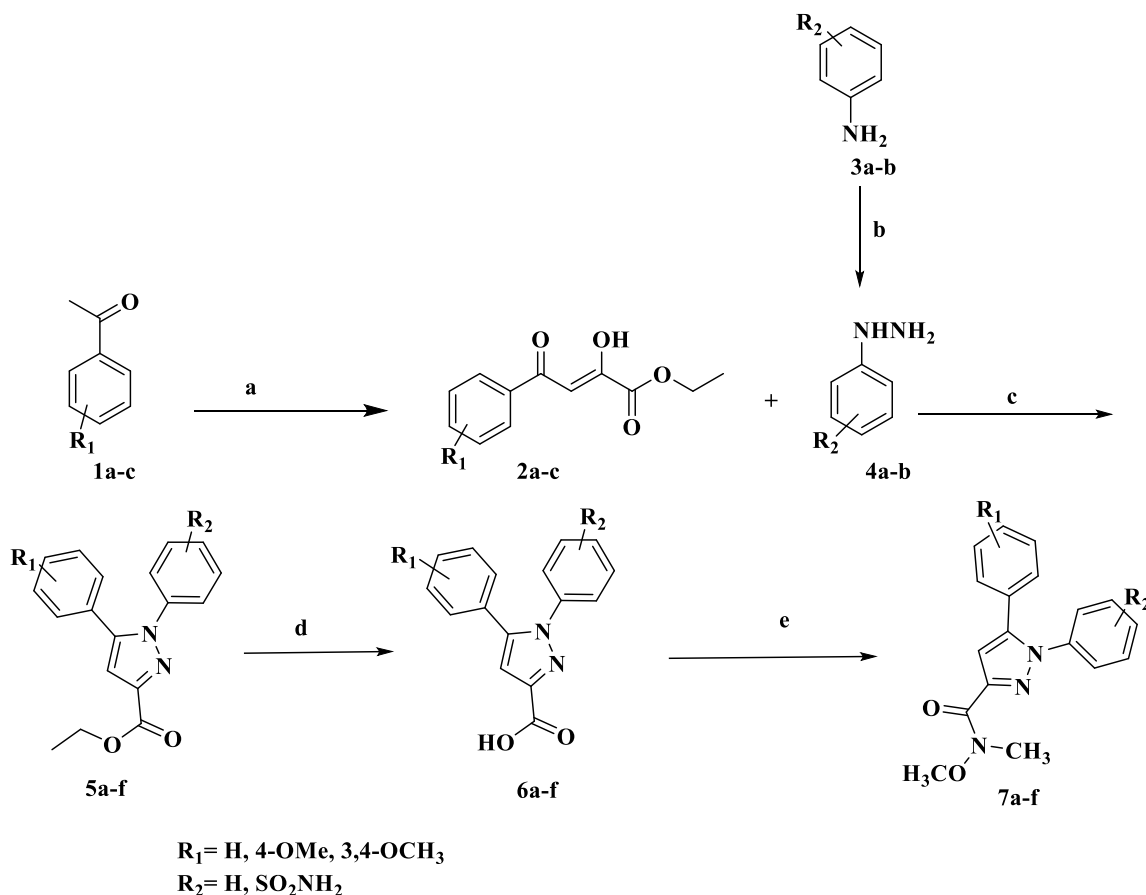
Reagent and conditions; a) diethyl oxalate, sodium ethoxide, absolute ethanol,4-6h; b) sodium nitrite, conc HCl, ice bath stirring, sodium sulphite, sodium hydroxide; c) sodium acetate, absolute ethanol, reflux for 2-3h; d) sodium hydroxide reflux for 3hr, HCl; e) EDC, HOBT, dry DMF, N,O-dimethyl hydroxylamine, DIPEA, stirring for 12 h.

Scheme1. **Synthetic route for target compounds 7a-f**.

2.2. Evaluation

2.2.1. In vitro antiproliferative activity

The newly synthesized compounds were evaluated for *in vitro* anticancer activity against different five cancer cell lines namely, human colorectal adenocarcinoma cell lines DLD1, human cervical cancer cell line Hela, human pancreatic cancer cell line Suit-2, human myelogenous leukemia cell line K562 and human hepatocellular carcinoma cell line HepG2 using WST-8 assay[23]. All compounds are screened on the five-cell line at concentration 100 µM to investigate the growth inhibition percent (GI%) induced by each compound using **Daunorubicin** as reference drug. Compound **7a** showed the highest (GI%) against all cell lines in comparison to remaining five compounds. As illustrated in **Table 1,** compound **7a** exhibited high GI% against Hela cell (95%), HepG2 (86%) and DLD1(83%). It showed moderate activity against Suit-2 (82%) and K562 (55%). This indicated that the un-substitution form of diarylpyrazole hybrid with *N,O*-dimethyl hydroxamate is more cytotoxic than the polar substitution. Also, Compound **7b** displayed good cytotoxicity against Suit-2 cell line with GI% of 83 and moderate activity against Hela cell line with GI% of 70, while the remining three cell line showed weak activities. Also, compound **7c** exhibited good activity against Hela cell line and Suit-2 cell line with GI% 84 on two cells and moderate activity against DLD1 and HepG2 with GI% 66 and 52 respectively, which indicate that 3,4-dimethoxy substitution is better than

4-OCH$_3$ in acetophenone moiety of diarylpyrazole. Furthermore, compounds **7d,7e** and **7f** that contain sulphamoyl moiety in phenyl hydrazine exhibited only moderate activity against Suit-2 cell line with GI% 66, 74 and 72, respectively. They exhibited weak activity in the remaining four cell line except compound **7f**, which exhibited moderate activity against K562 cell line with GI% 64, This indicated that the design rational for incorporation of sulphamoyl moiety into phenyl hydrazine is less good than unsubstituted phenyl hydrazine in these diarylpyrazole derivatives (**Fig. 4**).

For further investigation of compound **7a**, the GI% of compound **7a** was measured at different six concentrations 1, 10, 20, 50, 80, 100 µM and its IC$_{50}$ against DLD1, Hela and HepG2 cell lines was detected. For compound **7a** it showed moderate activity against DLD1, HepG2 cell lines with IC$_{50}$ = 69.6, 78.8 µM respectively. While it exhibited good activity against Hela cell line with IC$_{50}$ = 16 µM (**Table 2**) and (**Fig. 5**). From this data compound **7a** can be considered as antiproliferative agent against cervical cell cancer Hela cell line.

Table1. GI% of compounds **7a-f** at 100 µM against five cancer cell lines.

Compound	R_1	R_2	DLD-1	Hela	Suit-2	K562	HepG2
7a	H	H	83	95	82	55	86
7b	4-OCH$_3$	H	40	70	83	16	19
7c	3,4-OCH$_3$	H	66	84	84	45	52
7d	H	SO$_2$NH$_2$	39	NI	66	46	NI
7e	4-OCH$_3$	SO$_2$NH$_2$	48	28	74	4	25
7f	3,4-OCH$_3$	SO$_2$NH$_2$	25	NI	72	64	NI
Daunorubicin			84	100	92	100	100

NI= no inhibition
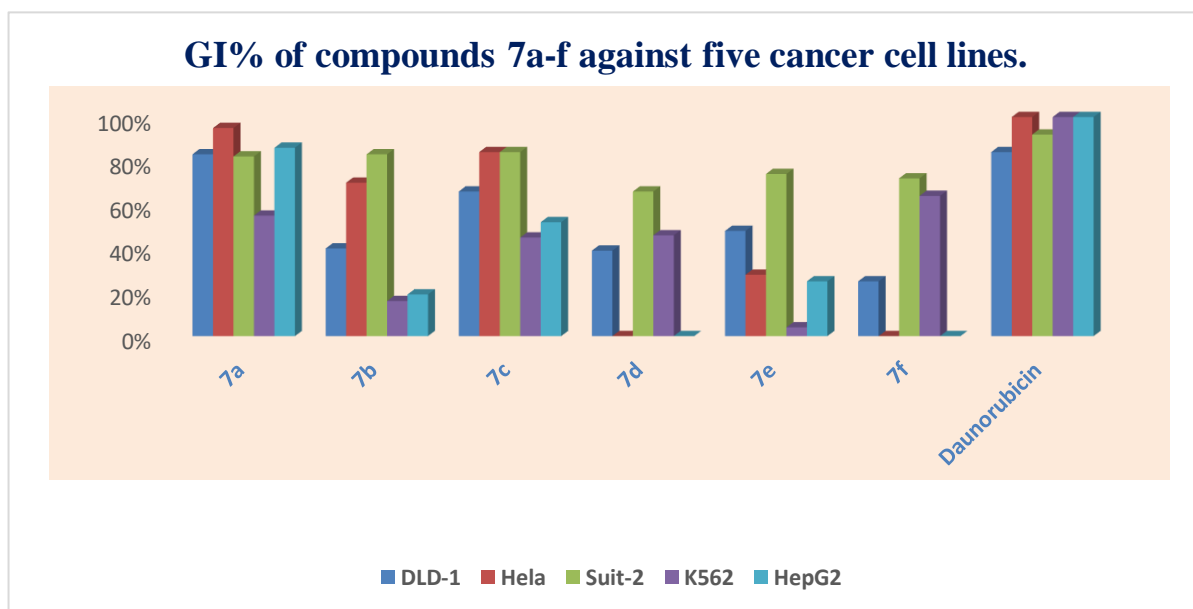
Figure 4: Percentage growth inhibition of DLD-1, Hela, Suit-2, K562 and HepG2 cell lines treated with compounds **7a-f** and **Daunorubicin** at concentration 100 µM.

Table 2. IC$_{50}$ (µM) of compound **7a** against DLD-1, Hela and HepG2 cell lines.

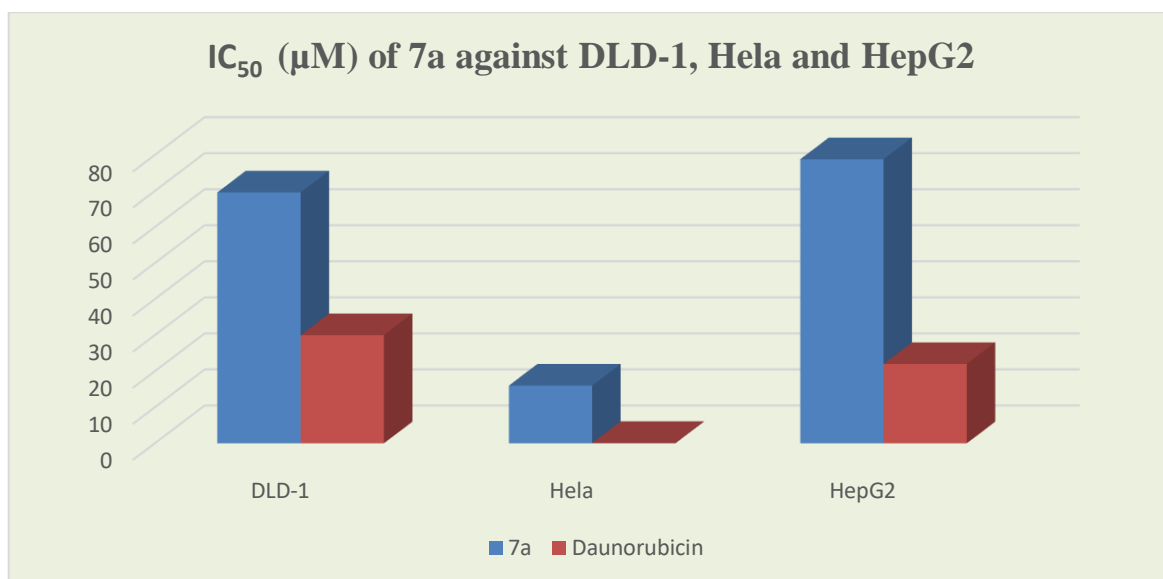| Compound	DLD-1	Hela	HepG2
7a	69.6	16	78.8
Daunorubicin	30	0.097	22

Figure 5: *In vitro* antiproliferative activity of compound **7a** and **Daunorubicin** against DlD-1, Hela and HepG2 cell lines as IC_{50} values.
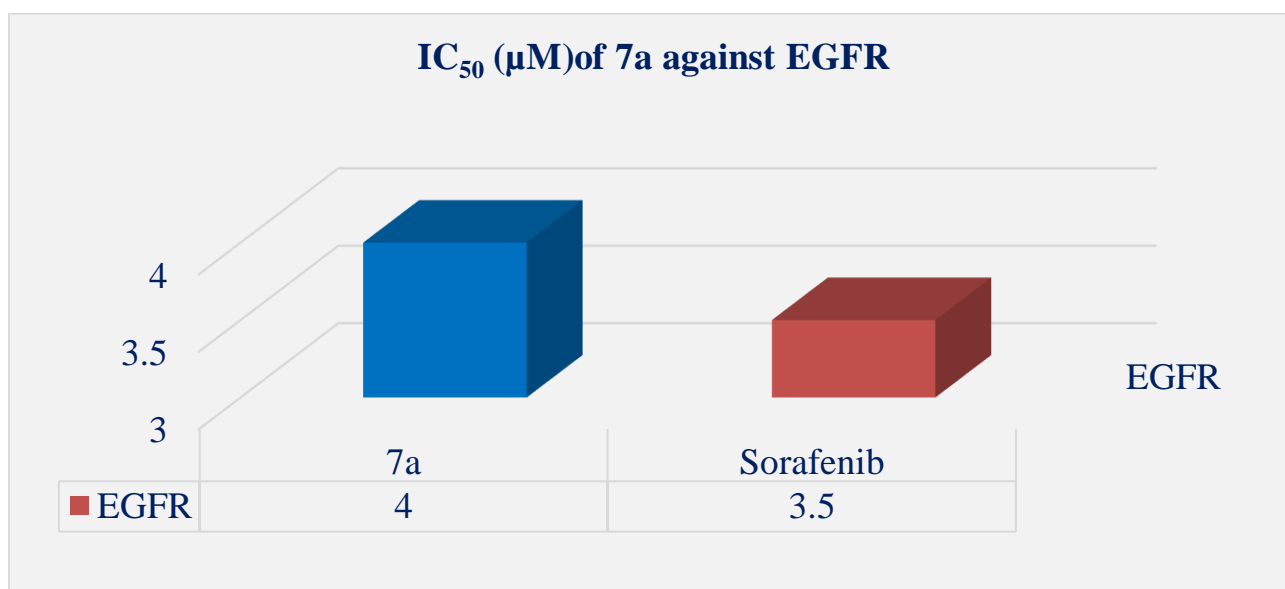

Figure 6: EGFR inhibitory activity of compound **7a** and **sorafenib**.

2.2.2. Inhibition of Epidermal growth factor activity (EGFR-TK)

Human EGFR-TK Elisa kit assay was performed to assess the EGFR inhibitory potency of compound **7a** using **sorafenib** as reference drug. Compound **7a** exhibited a potent inhibition to EGFR with IC_{50} = 4.00 µM, which is comparable to positive reference drug **Sorafenib** (IC_{50} = 3.5 µM). The result from this assay complements the finding of cancer cell- based assay and *in silico* studies, which indicates that antiproliferative activity of compound **7a** is mainly due to EGFR inhibition (**Fig. 5**).

2.2.3. In-silico molecular docking studies

For mechanistic investigation of antiproliferative activity of compound **7a,** we investigated it is in silico simulation on EGFR and JNK-2 enzyme. The investigation was done using sorafenib, a multitarget kinase inhibitor drug as reference.

2.2.3.1. EGFR docking

EGFR is a transmembrane tyrosine kinase receptor with important roles in vital cellular processes[24, 25]. EGFR signaling interruptions were shown to be linked with many diseases like cancer which later was identified as an oncogene [26]. So that, it was implicated as a crucial drug target by different therapeutic approaches including antibodies and small molecules. Thus, we aimed to develop a new class of small molecule inhibitors targeting EGFR kinase domain (**Fig.7**) [27]. In this study, we checked the virtual binding mode of **7a** which differentially bound the active site strongly than sorafenib that has a weaker tendency (Table 3). Although the phenyl ring of **7a** makes a van der Waals interaction with P794 (Fig. 4), sorafenib makes weaker hydrophobic interaction with the same residue (Fig. 5). Additionally, **7a** carbonyl group makes two van der Waals interactions at Q791 and L792 residues, while N-methyl interacts with C775. Importantly, the amine group of M793

residue acts as a hydrogen donor that forms hydrogen bonding with the carbonyl groups of both **7a** and sorafenib. The sandwiching effect was achieved by the hydrophobic contacts formed by the non-polar residues L718, V726, A743 and L792. Altogether, **7a** occupies the active site more tightly than sorafenib because its structurally compatible to the biding site more than sorafenib. It has been shown that the 2-pyridinecarboxamide group aggressively flipped to fit the binding site. This, in turn, results in a lower binding energy of **7a,** that was enhanced by the van der Waals interactions, than that of sorafenib. Hence, we deduced that the antiproliferative activity of **7a** is mainly due to EGFR inhibition.
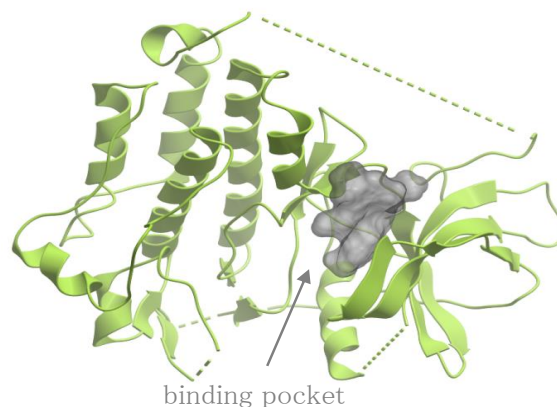

Figure 7: Ribbon representation of EGFR showing the binding pocket by a gray skin mesh (PDB ID: 4ZAU)[27].
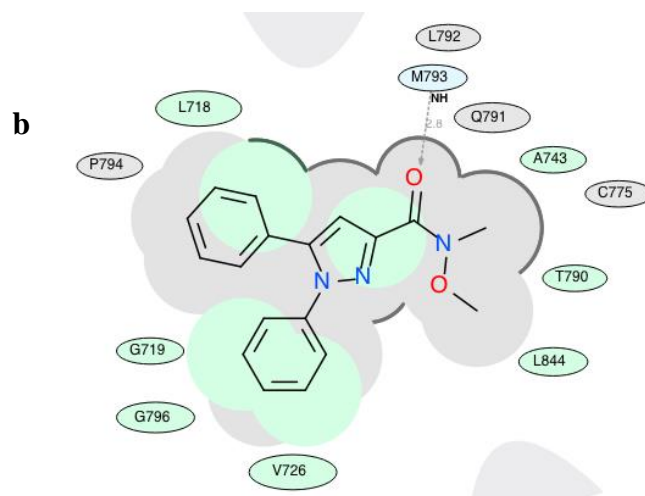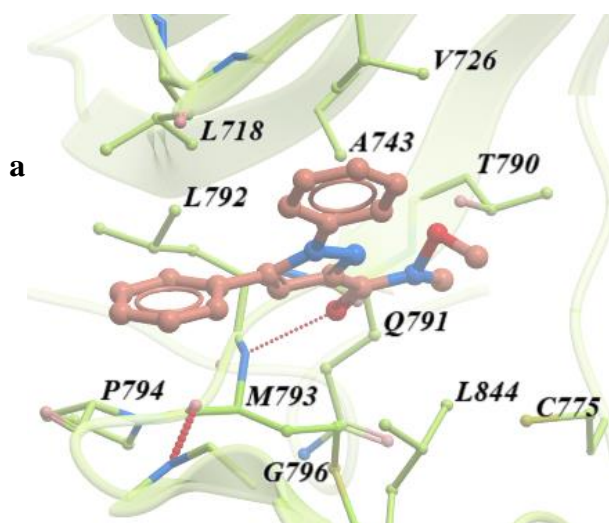

Figure 8: Docking pose of **7a** at the EGFR binding pocket. **a**, binding of **7a** (pink) to EGFR (light green) showing the interactive residues. Inter- and intra-molecular hydrogen bonds are shown as red dots. **b**, The corresponding 2D representation of **7a** at the binding pocket. Light green highlight is for hydrophobic interactions, light blue highlight is for hydrogen bonding (shown as dashed arrow) and gray highlight is for van der Waals interactions.
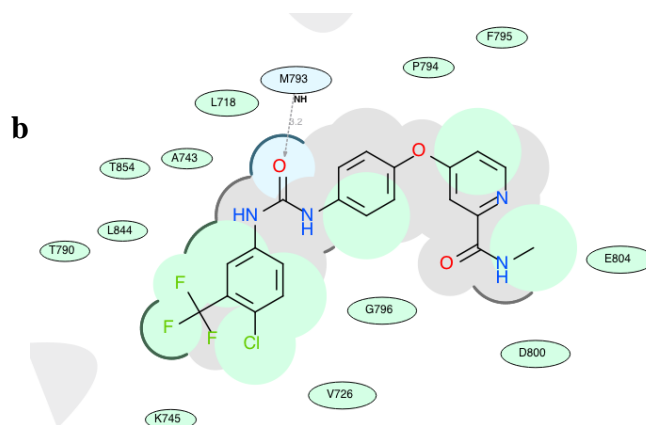

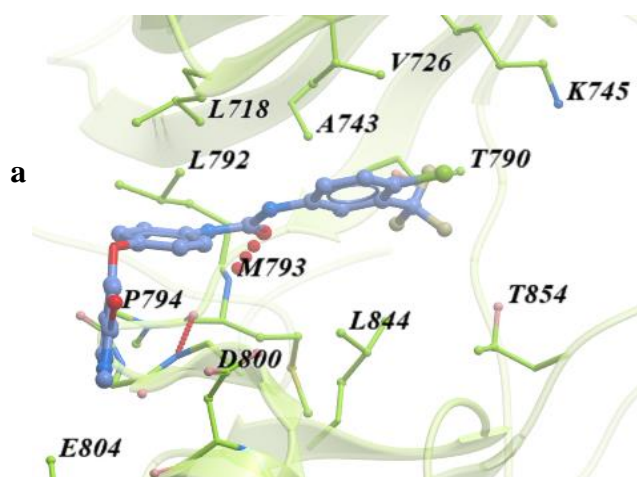**Figure 9:** Docking pose of Sorafenib at the EGFR binding pocket. **a**, binding of sorafenib (blue) to EGFR (light green) showing the interactive residues. Hydrogen bonds are shown as red dots. **b**, The corresponding 2D representation of sorafenib at the binding pocket. Light green highlight is for hydrophobic interactions and light blue highlight is for hydrogen bonding (shown as dashed arrow).

Table 3. Calculated binding properties of **7a** and Sorafenib against EGFR and JNK2.

Properties	Binding score		Hydrogen bonding energy (Kcal/mol)		Hydrophobic interaction energy (Kcal/mol)		Van der Waals interaction energy (Kcal/mol)	
Target receptor	JNK2	EGFR	JNK2	EGFR	JNK2	EGFR	JNK2	EGFR
Sorafenib	-49.83	-19.63	-6.67	-2.52	-10.38	-7.12	-	-
7a	-17.52	-21.52	-	-1.90	-7.26	-6.24	-29.85	-24

2.2.3.2. JNK-2 docking

JNK-2 is a member of MAP kinases family involved in signaling pathways which has been implicated in several diseases like cancer and inflammatory diseases[13]. So, this family is widely considered for targeting by small molecule therapeutics[14]. Inhibitors were classified into two types based on the binding target at the DFG conformations (aspartate-phenylalanine-glycine) of the activation loop[14, 28]. Type I inhibitors which targets DFG-in conformation and type II inhibitors that target DFG-out conformation, with a more respect to type II higher selectivity than type I. This is because the DFG-out conformation prevents the recruitment of ATP to the enzyme active site. This reveals that JNK2 can be inactivated by targeting DFG-out conformation[28]. Based on this, we docked the selected compounds against a pre-defined DFG-out conformation of JNK2 (**Fig. 10**) [14].

Since sorafenib is a common multitarget kinase (including MAP kinase) inhibitor, it showed to have higher binding affinity to JNK-2 active site, while **7a** structural non-compatibility and hydrophobicity resulted in a weaker binding affinity (**Table 3**). Unlike sorafenib, **7a** lacks hydrogen bonding at the active site as it makes hydrophobic interactions with D169 and F170 of DFG-out conformation with additional van der Waals interactions with the nonpolar residues E73, E109 and M111 (**Fig. 11**). Sorafenib extends at the active site from the hinge region (L110 and M111) to the base of c-helix (L76 and L77) which makes it structural compatible to fit the active site (**Fig. 12**). However, **7a** positions between the hinge region (M111) until the DFG-out conformation where the probability to inhibit JNK2 activity might be possible.
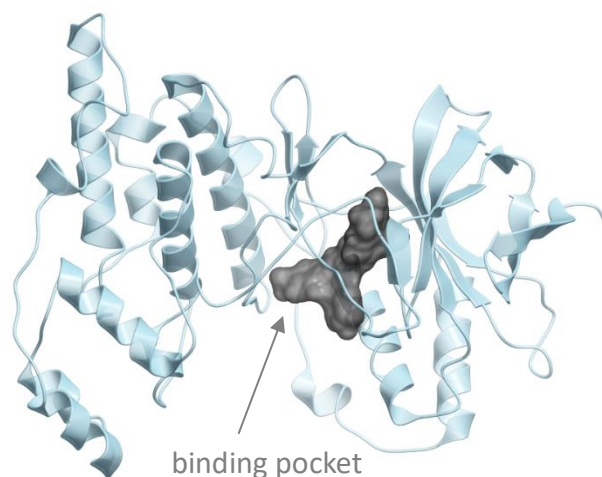

Figure 10: Ribbon representation of JNK2 showing the binding pocket by a gray skin mesh (PDB ID: 3NPC) [14].

3.Experimental

3.1. Chemistry

3.1.1. Materials and measurements

Solution phase reactions were monitored by thin layer chromatography (Merck Silica gel 60 F254) on glass plates and visualized with a UV lamp (254 nm) or with *p*-anisaldehyde and heating. Column chromatography was performed using spherical, neutral silica gel of diameter 40-100 μm (Kanto chemical co. Inc., Tokyo, Japan). 1H (400 or 500 MHz) and 13C NMR (100 or 125 MHz) spectra were recorded on either a JNM-ECX400 or JNM-ECX500 (JEOL, Tokyo, Japan). Chemical shifts are reported in ppm relative to tetramethylsilane (0 ppm), chloroform (7.26 ppm: 1H, 77.1 ppm: 13C) and dimethyl sulfoxide (2.50 ppm: 1H, 39.6 ppm: 13C). IR spectra were recorded at FT/IR-Spectrum Two (PerkinElmer, MA, USA). Mass spectra (ESI-MS) were carried out using the AccuTOF JMS-T100LC (JEOL, Tokyo, Japan). Melting points were recorded at a ATM-02 (AS ONE, Tokyo, Japan). For the cytotoxicity evaluation microplate reader, an MTP-310 absorbance microplate reader (CORONA, Hitachi-Naka, Japan) was used to measure the absorbance at wavelengths of 450 nm and 630 nm. All spectral measurement, melting point, cytotoxicity and EGFR inhibitory assay were performed in Department of Biochemical engineering, Faculty of Engineering, Yamagata university, Japan.

3.1.2. General procedure for synthesis of ethyl 4-(substituted phenyl)-2-hydroxy-4-oxobut-2-enoates 2a-c:

Ethanol (100 mL) was converted to sodium ethoxide by portion wise addition of sodium (0.46 g, 0.02 mol) before a solution of diethyl oxalate (2.92 g, 0.02 mol) and substituted acetophenone derivative (0.01 mol) in ethanol (50 mL) was added dropwise at 50 °C. The reaction mixture was heated under reflux for 2-3 h. After cooling the solvent was removed and the residue was taken up in water (200 mL) and acidified with concentrated HCl (1 mL). The aqueous mixture was extracted with ethyl acetate (3x150 mL). The combined extracts were washed with brine (100 mL), dried over anhydrous MgSO4, and concentrated. The obtained solid was recrystallized from methanol to give compounds **3a-c**[29, 30].
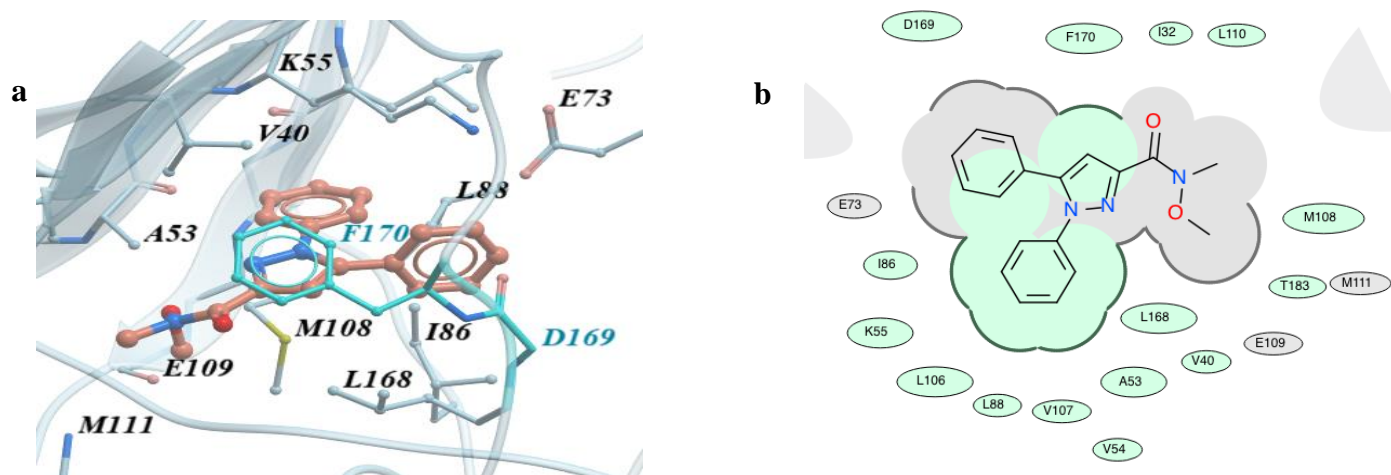
Fig. 11. Docking pose of **7a** at the JNK2 binding pocket. **a**, Binding of **7a** (pink) to JNK2 (sky blue) showing the interactive residues. DFG-out conformation highlighted in cyan. **b**, The corresponding 2D representation of **7a** at the binding pocket of JNK2. Light green highlight is for hydrophobic interactions and gray highlight is for van der Waals interactions.
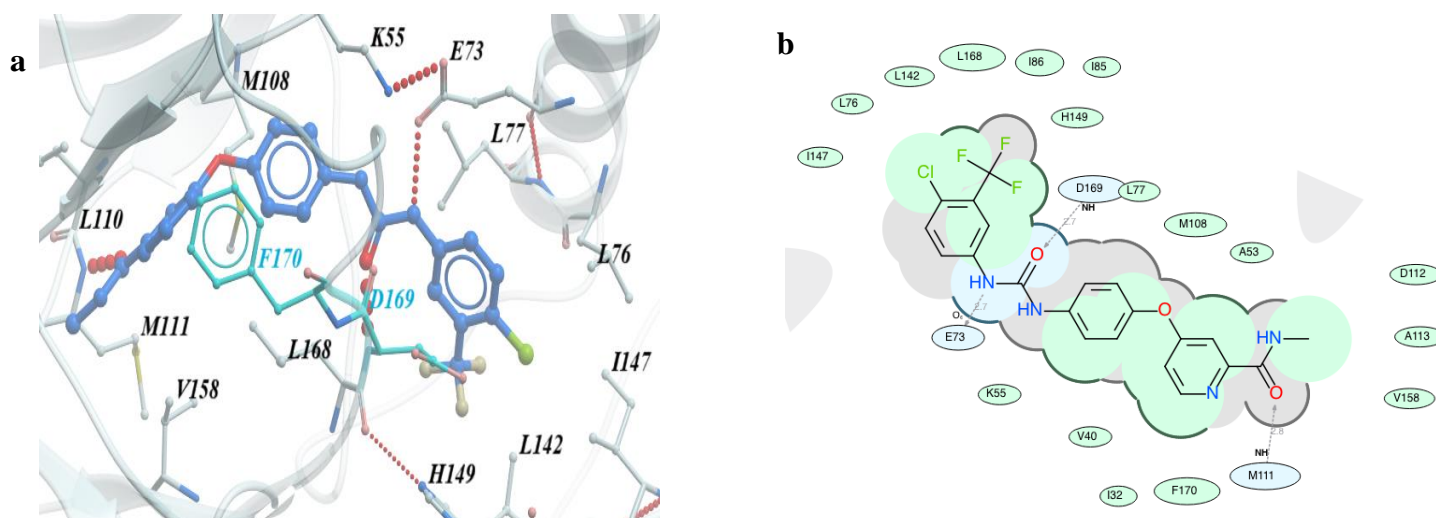

Fig. 12. Docking pose of sorafenib at the JNK2 binding pocket. **a**, binding of sorafenib (blue) to JNK2 (sky blue) showing the interactive residues. DFG-out conformation highlighted in cyan and hydrogen bonds shown as red dots. **b**, The corresponding 2D representation of sorafenib at the binding pocket of JNK2. Light green highlight is for hydrophobic interactions and light blue highlight is for hydrogen bonding (shown as dashed arrow).

3.1.3. General procedure for synthesis of 4-hydrazineylbenzenesulfonamide hydrochloride 3b:

A cold, stirred mixture of sulfanilamide (3.42 g, 0.02 mol), hydrochloric acid (10 mL) and crushed ice (200 g) was diazotized by the dropwise addition of sodium nitrite (1.4 g, 0.02 mol) in water (25 mL) over 30 min. The cold diazonium salt solution thus formed was rapidly added to a well-cooled solution of sodium sulphite (2.52 g) and sodium hydroxide (0.800g) in water (50 mL) with vigorous stirring, and the resulting mixture was left in the ice box for 15 minutes then acidification with 10 ml HCl and concentrated. The precipitated 4-hydrazineylbenzenesulfonamide hydrochloride was collected under reduced pressure and dried: white crystals; mp 225 °C (lit. mp 225 °C); yield 3.9 g (88%)[31].

3.1.4. General procedure for synthesis of Ethyl 1,5 diarypyarzole-3-carboxylate 5a-c:

A mixture of diketoesters **2a-c** (0.001mole) and phenylhydrazine (0.001mole) **4a** was dissolved in suitable amount of absolute ethanol (40 ml) and refluxed for 5 h. The reaction process was monitored by TLC using chloroform: methanol (95: 5) solvent system. The content of reaction mixture was evaporated under vacuum and crude product was purified by column chromatography [32].

Ethyl 5-diphenyl-1*H*-pyrazole-3-carboxylate (5a): Reddish brown powder; yield (0.220g, 75%); mp: 85- 87°C (lit. 82-84°C) [32].

Ethyl 5-(4-methoxyphenyl)-1-phenyl-1*H*-pyrazole-3-carboxylate (5b): Reddish brown powder; yield (0.280g, 81%); mp: 97- 99 °C (lit. 97-98°C)[33].

Ethyl 5-(3,4-dimethoxyphenyl)-1-phenyl-1*H*-pyrazole-3-carboxylate (5C): Brown powder, yield (0.220g, 63%); mp: 174- 176 °C (lit. 177 - 178°C) [29].

3.1.5. General procedure for synthesis of Ethyl 5-aryl-1-(4-sulfamoylphenyl)-1*H*-pyrazole-3- carboxylate (5d-f):

A mixture of diketoesters **2a-c** (0.001mole) and 4-hydrazineylbenzenesulfonamide hydrochloride (0.001mol) **4a** was dissolved in suitable amount of absolute ethanol (40 ml), sodium acetate (0.002 mol) was added, and reaction mixture was refluxed for 5 hr. The reaction process was monitored by TLC using chloroform: methanol (95: 5) solvent system. The content of reaction mixture was cooled, filtrated and the filtrate was evaporated under vacuum and crude product was purified by column chromatography[34].

Ethyl 5-phenyl-1-(4-sulfamoylphenyl)-1*H*-carboxylate (4d): Reddish powder; yield (0.245g, 66%), mp**:** 192-194 °C (lit. 192-194°C)[34].

Ethyl 5- (4-methoxyphenyl)-1-(4-sulfamoylphenyl)-1*H*-pyrazole-3-carboxylate (4e): Reddish brown powder; yield (0.285g, 71%), mp: 207-209 °C (lit. 205-207 °C)[35].

Ethyl 5-(3,4-dimethoxyphenyl)-1-(4-sulfamoylphenyl)-1*H*-pyrazole-3-carboxylate (4f): Reddish brown powder; yield (0.275g, 64%); mp: 214- 215°C[36].

3.1.6. General procedure for synthesis of 1,5 diarypyrazole carboxylic acids (6a-f):

Potassium hydroxide (KOH, 20%, 10 mL) was added to a solution of compounds **5a-f** (0.001 mol) in methanol, few drops of water were added, and the mixture was stirred at 60 °C for 4 h. After cooling, the mixture was poured into water, acidified with hydrochloric acid solution (1 M) to PH = 3 and extracted with ethyl acetate (3×50 mL) and discarded the aqueous layer. The combined organic extracts were dried with" anhydrous MgSO$_4$. The organic solvent was evaporated under vacuum to obtain a solid products **6a-f** [32].

1,5-diphenyl-1*H*-pyrazole-3-carboxylic acid (6a): Brown powder; yield (0.220g, 84%), mp: 180-182°C (lit. 182-183°C)[32].

5-(4-methoxyphenyl)-1-phenyl-1*H*-pyrazole-3-carboxylic acid (6b): Reddish brown powder; yield (0.230g, 79%), mp: 192-195 °C (lit. 196-197 °C) [37].

5-(3,4-dimethoxyphenyl)-1-phenyl-1*H*-pyrazole-3-carboxylic acid (6c): Brown powder; yield (0.270g, 84%); mp: 213-214°C; ¹H-NMR (400 MHz, DMSO-*d₆*) δ (ppm): 7.52-7.94 (m, 5H, Ar-H), 7.39 (s, 1H, pyrazole, *H*-4), 6.68-6.94 (m, 3H, Ar-H), 3.79 (s, 3H, OCH$_3$), 3.77 (s, 3H, OCH$_3$); ¹³C NMR (100MHz, DMSO-*d₆*) δ (ppm): 163.36, 160.36, 145.81, 144.09, 142.55, 130.71, 128.76, 127.45, 126.47, 125.40, 122.05, 120.40, 115.26, 110.45, 56.23, 56.12; ESI-MS m/z [M+H]$^+$ for C$_{18}$H$_{17}$N$_2$O$_4$ calculated: 325.1183, found: 325.256.

5-phenyl-1-(4-sulfamoylphenyl)-1*H*-pyrazole-3-carboxylicacid (6d): Yellowish brown powder; yield (0.265g, 78%), mp: 184-186 °C (lit. 188.5-190.50 °C)[38].

5-(4-methoxyphenyl)-1-(4-sulfamoylphenyl)-1*H*-pyrazole-3-carboxylic acid (6e): Brownish powder; yield (0.270g, 73%), mp: 197-198 °C[30].

5-(3,4-dimethoxyphenyl)-1-(4-sulfamoylphenyl)-1*H*-pyrazole-3-carboxylic acid (6f): Reddish brown powder; yield (0.310g, 77%); mp: 206-208°C; ¹H-NMR (400 MHz, DMSO-*d6*) δ (ppm): 10.76 (s, 1H, OH), 7.99 (s, 1H, Ar-H), 7.91(d, *J*= 8.00Hz, 2H, Ar-H), 7.79 (d, *J*= 8.00 Hz, 2H, Ar-H), 7.60-7.65 (m, 4H, 2Ar-H+SO$_2$NH$_2$), 7.43 (s, 1H, pyrazole, *H*-4), 3.89 (s, 6H, 2 OCH$_3$);¹³C NMR (100MHz, DMSO-*d6*) δ (ppm): 163.36, 159.98, 147.36, 145.23, 141.21, 131.47, 130.17, 128.82, 126.87, 125.54, 122.87, 119.99, 115.14, 107.53, 56.38, 56.21; ESI-MS

m/z [M+H]$^+$ for C$_{18}$H$_{18}$N$_3$O$_6$S calculated: 404.0911, found: 404.0271.

3.1.7. General procedure for preparation of compounds 7a-f:
A mixture of pyrazole acid derivatives **6a-f** (0.001 mol), 1-Ethyl-3-(3-dimethylaminopropyl) carbodiimide hydrochloride (EDC) (0.002 mol), hydroxybenzotriazole (HOBT) (0.002 mol), were stirred in 5 ml dry DMF for 30 min then *N,N*-diisopropylethylamine (DIPEA) (0.002 mol) and *N,O*-dimethyl hydroxylamine hydrochloride (0.002 mol) were added to the mixture and stirred for 12 hrs. Then 20 ml of distilled water were added, followed by acidification with dil. HCl, extraction twice with ethyl acetate and purification were performed by using column chromatography with chloroform as eluent for compounds **7a-c** and chloroform: methanol 98:2 for compounds **7d-f**.

N-Methoxy-N-methyl-1,5-diphenyl-1*H*-pyrazole-3-carboxamide (7a): Yellowish brown solid; yield (0.163g, 63%); mp: 77-79 °C; IR (ATR) cm^{-1}: 1638 (C=O), 1595 (C=C aromatic); ¹H-NMR (500 MHz, CDCl$_3$) δ (ppm): 7.30-7.32 (m, 4H, Ar-H), 7.27-7.29 (m, 4H, Ar-H), 7.20-7.23 (m, 2H, Ar-H), 6.98 (s, 1H, pyrazole *H*-4), 3.84 (s, 3H, OCH$_3$), 3.49 (s,3H, NCH$_3$); ¹³C NMR (100MHz, DMSO-*d₆*) δ (ppm): 162.75, 146.31, 143.54, 139.11, 129.90, 129.01, 128.87, 128.65, 127.77, 125.02, 124.01, 110.97, 61.36, 36.23; HRMS: ESI-MS m/z [M$^+$Na] for C$_{18}$H$_{17}$N$_3$NaO$_2$ calculated: 330.1218, founded: 330.1245.

N-Methoxy-5-(4-methoxyphenyl)-N-methyl-1-phenyl-1*H*-pyrazole-3 carboxamide (7b): Yellowish brown solid; yield (0.200g, 59%); mp: 83-85 °C; IR (ATR) cm^{-1}: 1672 (C=O), 1597 (C=C aromatic); ¹H-NMR (500 MHz, CDCl$_3$) δ (ppm): 7.94 (d, *J*= 7.00 Hz, 2H, Ar-H), 7.92 (d, *J*= 7.00 Hz, 2H, Ar-H), 7.31-7.33 (m, 2H, Ar-H), 7.25 (s, 1H, pyrazole *H*-4), 6.90-6.94 (m, 4H, Ar-H), 3.86 (s, 3H, OCH$_3$), 3.82 (s, 3H, OCH$_3$), 3.54 (s, 3H, N CH$_3$); ¹³C NMR (100MHz, DMSO-*d₆*) δ (ppm): 163.76, 130.69, 130.63, 130.19, 129.33, 128.99, 127.98, 125.46, 114.00, 113.81, 113.33, 109.28, 60.89, 55.57, 34.15; HRMS: ESI-MS m/z [M+Na] for C$_{19}$H$_{19}$N$_3$NaO$_3$ calculated:360.1324, founded: 360.1311.

5-(3,4-Dimethoxyphenyl)-N-methoxy-N-methyl-1-phenyl-1*H*-pyrazole-3-carboxamide (7c): Yellowish brown solid; yield (0.200g, 54%); mp: 72-74 °C; IR (ATR) cm^{-1}: 1645 (C=O), 1595 (C=C aromatic); ¹H-NMR (500 MHz, CDCl$_3$) δ (ppm): 7.97 (s, 1H, Ar-H), 7.49 (d, 1H, *J* = 6.50 Hz, Ar-H), 7.28-7.33 (m, 5H, Ar-H), 6.93 (s, 1H, pyrazole *H*-4), 6.80 (d, *J* = 6.50 Hz, 1H, Ar-H), 3.90 (s, 3H, OCH$_3$), 3.85 (s, 3H, OCH$_3$), 3.82 (s, 3H, OCH$_3$), 3.59 (s, 3H, CH$_3$); ¹³C NMR (100MHz, DMSO-*d6*) δ (ppm): 163.78, 153.20, 149.51, 148.98, 143.54, 140.10, 130.53, 128.52, 127.79, 124.72, 121.60, 111.01, 109.37, 61.60, 55.93, 55.73, 36.56; HRMS: ESI-MS m/z [M$^+$Na] for C$_{20}$H$_{21}$N$_3$NaO$_4$ calculated: 390.1430, founded: 390.1439.

N-Methoxy-N-methyl-5-phenyl-1-(4-sulfamoylphenyl)-1*H*-pyrazole-3-carboxamide (7d): Yellowish brown solid; yield (0.196g, 51%); mp:77-79 °C; IR (ATR) cm^{-1}: 1627 (C=O), 1595 (C=C aromatic), 1158 (SO$_2$NH$_2$); ¹H-NMR (500 MHz, DMSO-*d₆*) δ (ppm): 7.83 (d, *J* = 8.5 Hz, 2H, Ar-H), 7.49 (d, *J* = 8.5 Hz, 2H, Ar-H), 7.47 (s, 2H, SO$_2$NH$_2$), 7.33-7.38 (m, 3H, Ar-H), 7.27-7.28 (m, 2H, Ar-H), 6.99 (s, 1H, pyrazole *H*-4), 3.72 (s, 3H, OCH$_3$), 3.34 (s, 3H, NCH$_3$); ¹³C NMR (100MHz, DMSO-*d6*) δ (ppm): 164.10, 146.32, 143.32, 141.47, 132.63, 129.57. 129.48, 129.30, 127.38, 126.06, 112.68, 109.93, 61.60, 35.90; HRMS: ESI-MS m/z [M$^+$Na] for C$_{18}$H$_{18}$N$_4$NaO$_4$S calculated: 409.0946, founded: 409.0950.

N-Methoxy-5-(4-methoxyphenyl)-N-methyl-1-(4-sulfamoylphenyl)-1*H*-pyrazole-3-carboxamide (7e): Yellowish brown solid; yield (0.200g, 48%); mp: 88-90°C; IR

(ATR) cm^{-1}: 1615 (C=O), 1590 (C=C aromatic), 1157 (SO$_2$NH$_2$); ^{1}H-NMR (500 MHz, DMSO-d_6) δ (ppm): 7.95 (d, J = 8.50 Hz, 2H, Ar-H), 7.67 (d, J = 8.5 Hz, 2H, Ar-H), 7.49 (s, 2H, SO$_2$NH$_2$), 7.38 (d, J = 7.6 Hz, 2H, Ar-H), 7.35 (d, J = 7.6 Hz, 2H, Ar-H), 6.92 (s, 1H, pyrazole H-4), 3.75 (s, 3H, OCH$_3$), 3.72 (s, 3H, OCH$_3$), 3.34 (s, 3H, NCH$_3$); ^{13}C NMR (100MHz, DMSO-$d6$) δ (ppm): 161.39, 145.28, 143.94, 141.88, 132.91, 131.20, 129.13, 128.12, 125.04, 119.92, 115.06, 110.62, 63.33, 56.15, 29.34; HRMS: ESI-MS m/z [M+Na] for C$_{19}$H$_{20}$N$_4$NaO$_5$S calculated: 439.1052, founded: 439.1025.

5-(3,4-Dimethoxyphenyl)-*N*-methoxy-*N*-methyl-1-(4-sulfamoylphenyl)-1*H*-pyrazole-3-carboxamide   (7f):
Yellowish brown solid; yield (0.227g, 51%); mp: 135-137 °C; IR (ATR) cm^{-1}: 1617 (C=O), 1590 (C=C aromatic), 1157 (SO$_2$NH$_2$); ^{1}H-NMR (500 MHz, DMSO-d_6) δ (ppm): 7.93 (d, J= 8.6 Hz, 2H, Ar-H), 7.91 (s, 1H, Ar-H), 7.87 (d, J = 8.50 Hz, 1H, Ar-H), 7.68 (d, J = 8.6 Hz,2H, Ar-H), 7.51 (s, 2H, SO$_2$NH$_2$), 7.36 (d, J = 7.6 Hz, 2H, Ar-H), 6.98 (s, 1H, pyrazole H-4), 6.91 (d, J = 8.50 Hz, 1H, Ar-H), 3.75 (s, 3H, OCH$_3$), 3.72 (s, 3H, OCH$_3$), 3.57 (s, 3H, OCH$_3$), 3.35 (s, 3H, NCH$_3$); ^{13}C-NMR (100MHz, DMSO-d_6) δ (ppm): 163.08, 149.73, 148.05, 143.32, 132.23, 129.33, 128.84, 126.12, 125.34, 119.63, 118.55, 110.13, 61.99, 55.99, 55.86, 30.35; HRMS: ESI-MS m/z [M$^+$H] for**2.** C$_{20}$H$_{23}$N$_4$O$_6$S calculated: 447.1333, founded: 447.1348.

3.2. Biological activity screening

3.2.1. *In vitro* antiproliferative activity

Cytotoxicity of compounds **7a-f** was evaluated by a standard water-soluble tetrazolium-8 (WST-8) assay. Five cell lines were maintained in a suspension culture of DMEM (Hela, Suit-2 and HepG2) or PRMI (DLD1, K562) supplemented with 5% FBS (Fetal Bovine Serum) containing 1% of a penicillin-streptomycin (1:1) mixture. A 100 µL aliquot of cells (10000 cells/mL) were added to a 96 well plate and incubated for 24 h at 37°C in a humidified incubator containing 5% CO$_2$ in air. After 24 h, a 10 µL aliquots of the compound (concentrations varying in the range of 10 - 150 µM) was added to each of the 96 wells and incubated for 24 h. A 10 µL WST-8 solution (mixture of WST-8 and 1-Methoxy PMS) was added to each well and the incubation continued for 3 h. The visible absorbance at 450 nm and 630 nm as the reference wavelength of each well was quantified using a microplate reader.

3.2.2. EGFR inhibitory assay

This assay employs the quantitative sandwich enzyme immunoassay technique. An antibody specific for EGFR has been pre-coated onto a microtiter plate. Standards or samples are pipetted into the wells and any EGFR present is bound by the immobilized antibody. After washing away any unbound substances, a biotin-conjugated antibody specific for EGFR is added to each well and incubate. Following a washing to remove unbound substances, streptavidin conjugated to Horseradish Peroxidase (HRP) is added to each microplate well and incubated. After washing away any unbound antibody-enzyme reagent, a substrate solution (TMB) is added to the wells and color develops in proportion to the amount of EGFR bound in the initial step. The color development is stopped by the addition of acid and the intensity of the color is measured at a wavelength of 450nm ±2nm. The concentration of EGFR in the sample is then determined by comparing the O.D of samples to the standard curve.

3.2.3. Docking

Docking simulation was performed by the Inter-coordinate Mechanics (ICM) using ICM-Pro 3.8 software (MolSoft L.L.C, USA)[39]. First, we generated the 3D structure of the **7a** and sorafenib (a reference MAP kinase inhibitor)[40] to perform well-suited docking. Then, we prepared the receptors by adjusting the interface properties including water molecules deletion, hydrogen atoms optimization and formal charges refinement. In addition, we logged receptors relaxation to run flexible docking. The ligands' binding affinities were calculated by the Gaussian potential based on the ligand electrostatic potential and shape complementarity at the binding site[14, 27]. In these studies, we used the template-docking method by selecting pre-defined binding pockets of the study receptors. For the Epidermal Growth Factor Receptor (EGFR), we built the structural models of the selected ligands against human EGFR complexed with AZD9291 inhibitor (2.80 Å; PDB ID: 4ZAU)[24]. For c-Jun N-terminal kinase 2 (JNK2), we used the crystal structure of wild type JNK2 complexed with the P38α inhibitor; BIRB796 (2.35 Å; PDB ID: 3NPC)[26].

Conclusion

A series of 1,5-diaryoyrazole-*N*,*O*-dimethylhdroxamate hybrid derivatives were synthesized and evaluated for their cytotoxicity against different cancer cell lines. Compound **7a** exhibited good antiproliferative activity against human cervical cancer Hela cell lines with IC$_{50}$ = 16 µM, and moderate activity against remaining four cell lines. Also, compound **7a** demonstrated a potent EGFR inhibitory activity with IC$_{50}$ = 4.00 µM in comparison to a reference drug sorafenib. In silico docking studies of compound **7a** showed that the binding affinity and fitting of compound **7a** on EGFR with total binding score is better than sorafenib, a multitarget kinase drug because of more Vander Waals binding interaction. In addition to, compound **7a** showed binding affinities to JNK-2 enzyme, which is one of MAP kinases and play an important role in tumorigenesis, which indicated that the antiproliferative activity of **7a** is due to inhibition of EGFR and JNK-2 activities.

References

[1]Gallorini, M., A. Cataldi, and V. di Giacomo, Cyclin-dependent kinase *modulators and cancer therapy.* BioDrugs, 2012. **26**(6): p. 377-391.
[2]Kibria, G., H. Hatakeyama, and H. Harashima, *Cancer multidrug resistance: mechanisms involved and strategies for circumvention using a drug delivery system.* Archives of pharmacal research, 2014. **37**(1): p. 4-15.
[3]Abdelgawad, M.A., et al., *Design, synthesis and antitumor activity of novel pyrazolo [3, 4-d] pyrimidine derivatives as EGFR-TK inhibitors.* 2016. **66**: p. 88-96.
[4]Mitsudomi, T. and Y.J.T.F.j. Yatabe, *Epidermal growth factor receptor in relation to tumor development: EGFR gene and cancer.* 2010. **277**(2): p. 301-308.
[5]Rego, R., et al., *Prognostic effect of activated EGFR expression in human colon carcinomas: comparison with EGFR status.* 2010. **102**(1): p. 165-172.
[6]Cao, C., et al., *Priming with EGFR tyrosine kinase inhibitor and EGF sensitizes ovarian cancer cells to respond to chemotherapeutical drugs.* 2008. **266**(2): p. 249-262.

[7]Bridges, A.J.C.m.c., *The rationale and strategy used to develop a series of highly potent, irreversible, inhibitors of the epidermal growth factor receptor family of tyrosine kinases.* 1999. **6**(9): p. 825-844.

[8]Butterworth, S., et al., *The structure-guided discovery of osimertinib: the first US FDA approved mutant selective inhibitor of EGFR T790M.* 2017. **8**(5): p. 820-822.

[9]Keter, F.K. and J. Darkwa, *Perspective: the potential of pyrazole-based compounds in medicine.* Biometals, 2012. **25**(1): p. 9-21.

[10]Kumar, V., et al., *Pyrazole containing natural products: synthetic preview and biological significance.* European journal of medicinal chemistry, 2013. **69**: p. 735-753.

[11]Çalışkan, B., et al., *Synthesis and evaluation of analgesic, anti-inflammatory, and anticancer activities of new pyrazole-3 (5)-carboxylic acid derivatives.* Medicinal Chemistry Research, 2013. **22**(2): p. 782-793.

[12]Yuan, J.-W., et al., *Synthesis and biological evaluation of compounds which contain pyrazole, thiazole and naphthalene ring as antitumor agents.* 2014. **24**(10): p. 2324-2328.

[13]Shaw, D., et al., *The crystal structure of JNK2 reveals conformational flexibility in the MAP kinase insert and indicates its involvement in the regulation of catalytic activity.* Journal of molecular biology, 2008. **383**(4): p. 885-893.

[14].Kuglstatter, A., et al., *X-ray crystal structure of JNK2 complexed with the p38α inhibitor BIRB796: insights into the rational design of DFG-out binding MAP kinase inhibitors.* Bioorganic & medicinal chemistry letters, 2010. **20**(17): p. 5217-5220.

[15]Abdelrahman, K.S., et al., *JNK signaling as a target for anticancer therapy.* 2021: p. 1-30.

[16]Wong, B.C.-y., et al., *Cyclooxygenase-2 inhibitor (SC-236) suppresses activator protein-1 through c-Jun NH2-terminal kinase.* 2004. **126**(1): p. 136-147.

[17]Burnette, B.L., et al., *SD0006: a potent, selective and orally available inhibitor of p38 kinase.* 2009. **84**(1): p. 42-60.

[18]Viegas-Junior, C., et al., *Molecular hybridization: a useful tool in the design of new drug prototypes.* Current medicinal chemistry, 2007. **14**(17): p. 1829-1852.

[19]Chen, J., et al., *Discovery of a novel rhein-SAHA hybrid as a multi-targeted anti-glioblastoma drug.* 2019: p. 1-10.

[20]Zhan, P., et al., *Medicinal chemistry insights into novel HDAC inhibitors: an updated patent review (2012-2016).* 2017. **12**(1): p. 16-34.

[21]Bechmann, N., et al., *Novel (pyrazolyl) benzenesulfonamides with a nitric oxide-releasing moiety as selective cyclooxygenase-2 inhibitors.* Bioorganic & medicinal chemistry letters, 2015. **25**(16): p. 3295-3300.

[22]Sidique, S., et al., *Design and synthesis of pyrazole derivatives as potent and selective inhibitors of tissue-nonspecific alkaline phosphatase (TNAP).* Bioorganic & medicinal chemistry letters, 2009. **19**(1): p. 222-225.

[23]Shin, U.c., et al., *Development of a 68Ga‐labelled PET tracer for carbonic anhydrase IX‐overexpressed tumors using the artificial sweetener saccharin.* Journal of Labelled Compounds and Radiopharmaceuticals, 2020.

[24]Hynes, N.E. and H.A. Lane, *ERBB receptors and cancer: the complexity of targeted inhibitors.* Nature Reviews Cancer, 2005. **5**(5): p. 341-354.

[25]Sogabe, S., et al., *Structure-based approach for the discovery of pyrrolo [3, 2-d] pyrimidine-based EGFR T790M/L858R mutant inhibitors.* ACS medicinal chemistry letters, 2013. **4**(2): p. 201-205.

[26]Zhang, H., et al., *ErbB receptors: from oncogenes to targeted cancer therapies.* The Journal of clinical investigation, 2007. **117**(8): p. 2051-2058.

[27]Yosaatmadja, Y., et al., *Binding mode of the breakthrough inhibitor AZD9291 to epidermal growth factor receptor revealed.* Journal of structural biology, 2015. **192**(3): p. 539-544.

[28]Pargellis, C., et al., *Inhibition of p38 MAP kinase by utilizing a novel allosteric binding site.* Nature structural biology, 2002. **9**(4): p. 268-272.

[29]Radwan, A.A., et al., *Novel ethyl 1, 5-disubstituted-1H-pyrazole-3-carboxylates as a new class of antimicrobial agents.* 2014. **64**(3): p. 335-344.

[30]Li, Z., et al., *Design, synthesis and evaluation of novel diaryl-1, 5-diazoles derivatives bearing morpholine as potent dual COX-2/5-LOX inhibitors and antitumor agents.* 2019. **169**: p. 168-184.

[31]Soliman, R.J.J.o.m.c., *Preparation and antidiabetic activity of some sulfonylurea derivatives of 3, 5-disubstituted pyrazoles.* 1979. **22**(3): p. 321-325.

[32]Aghazadeh Tabrizi, M., et al., *Discovery of 1, 5-diphenylpyrazole-3-carboxamide derivatives as potent, reversible, and selective monoacylglycerol lipase (MAGL) inhibitors.* 2018. **61**(3): p. 1340-1354.

[33]Murray, W.V. and M.P.J.J.o.h.c. Wachter, *A simple regioselective synthesis of ethyl 1, 5‐diarylpyrazole‐3‐carboxylates.* 1989. **26**(5): p. 1389-1392.

[34]Yamali, C., et al., *Synthesis, biological evaluation and in silico modelling studies of 1, 3, 5-trisubstituted pyrazoles carrying benzenesulfonamide as potential anticancer agents and selective cancer-associated hCA IX isoenzyme inhibitors.* 2019. **92**: p. 103222.

[35]Rogez-Florent, T., et al., *New selective carbonic anhydrase IX inhibitors: synthesis and pharmacological evaluation of diarylpyrazole-benzenesulfonamides.* 2013. **21**(6): p. 1451-1464.

[36]Lu, X.-Y., et al., *Coumarin sulfonamides derivatives as potent and selective COX-2 inhibitors with efficacy in suppressing cancer proliferation and metastasis.* 2016. **26**(15): p. 3491-3498.

[37]Raiford, L.C. and E.L.J.J.o.t.A.C.S. Hill, *Effect of Constitution on the Rearrangement of the Phenylhydrazones of Some Unsymmetrically Substituted Dibenzalacetones1.* 1934. **56**(1): p. 174-176.

[38]Hwang, S.H., et al., *Synthesis and structure− activity relationship studies of urea-containing pyrazoles as dual inhibitors of cyclooxygenase-2 and soluble epoxide hydrolase.* 2011. **54**(8): p. 3037-3050.

[39]Neves, M.A., M. Totrov, and R. Abagyan, *Docking and scoring with ICM: the benchmarking results and strategies for improvement.* Journal of computer-aided molecular design, 2012. **26**(6): p. 675-686.

[40]An, J., M. Totrov, and R. Abagyan, *Pocketome via comprehensive identification and classification of ligand binding envelopes.* Molecular & Cellular Proteomics, 2005. **4**(6): p. 752-761.